Permeability and permittivity spectra of granular materials

Craig A. Grimes
Lockheed Research Laboratories, 3251 Hanover Street, G91-60, Palo Alto, California 94304

Dale M. Grimes
Crale Inc., 504 West 24th, Austin, Texas 78705

(Received 21 May 1990; revised manuscript received 6 November 1990)

We present an extended analytic technique for calculating the permeability and permittivity spectra of granular materials. It addresses the relationship between grain properties, their size relative to the wavelength, and the permeability and permittivity spectra of polycrystalline material. The scattered multipolar fields about a single sphere are related to the polarizability of an ordered congregation of such spheres. The product of the external wave vector k and sphere radius a is small and the product of the internal wave vector k_i and a unrestricted. The Clausius-Mossotti relation is used in combination with the scattering results to yield an equation that permits us to calculate the effective permeability and permittivity spectra of a cubic array. The result is a variety of possible spectral types, including complex permittivity and permeability spectra that have been measured and explained either by including multiple atomic-level sources or by statistical weighting over an ensemble of grains. This theory predicts both "classical" and "anomalous" spectra from a single source, as well as certain conglomerate permeability spectra that have been measured and for which no direct explanation is available. Our results show that an understanding of the permeability and permittivity spectra of composite materials cannot be complete without inclusion of a dependence on the ratio of the grain size to the wavelength.

I. INTRODUCTION

Electronic materials, chosen for having specific values of relative permittivity and permeability, are widely used and have in common an inherent frequency dependence. The sources of the permittivity and permeability are thought to be atomic-scale dipoles.[1] By definition the permeability and permittivity are, respectively, the derivative of the magnetization M with respect to the magnetic field and the derivative of the polarization P with respect to the electric field. M and P are the (vectorial) sums, respectively, of all magnetic- and electric-dipole moments per unit volume.

Magnetization changes due to domain-wall motion are calculated with use of the lossy harmonic-oscillator equation. A dual procedure is used for the induced permittivity. Magnetization changes due to coherent rotation are calculated with use of the electromagnetic torque equation, usually with a phenomenologically added Gilbert or Landau-Lifshitz loss term for magnetics. A similar technique with a Debye loss term is used for dielectrics. Although spectra calculated with use of these techniques match quite well the measured spectra of such ideal materials as single crystals, changing the parameters of the model only smooths or sharpens the shape of the resonance, raises or lowers the resonance frequency, or raises or lowers the magnitude of the initial component. The techniques cannot explain multiply peaked spectra of uniform, polycrystalline material.

The purpose of this paper is to extend the present analytic technique for calculating permeability and permittivity spectra and to apply the results to solid, polycrystalline materials.[2-6] Our results show that a single microscopic source can result in a broad range of macroscopic permeability and permittivity spectra and that the permeability and permittivity are interdependent. Our calculations show spectral forms that include resonances, relaxations, and anomalous forms.[7-10]

We begin by solving for the scattered and internal fields, respectively, about and within a dielectric sphere of arbitrary scalar permittivity and permeability that is illuminated by an incident electromagnetic plane wave. The product of the wave vector k and sphere radius a is much less than 1 and the product of the internal wave vector k_i and sphere radius, $k_i a = ka\sqrt{\mu\epsilon}$, is unconstrained. The field coefficients are determined from matching boundary conditions on the surface of the sphere and related to the dipole moment. We then form a polycrystalline solid by bringing together an infinite set of such spheres to form a cubic array. Sphere-sphere interactions are calculated with the help of the Clausius-Mossotti equation.

We justify applying the technique to sources arising from electromagnetic torque by requiring the initial magnetization (polarization) of the grains to be random; then the sum over nearest-neighbor off-diagonal terms is zero and can be ignored.[11,12] This allows us to assign to the individual spheres scalar properties derived from either, or both, induced and existent dipole moments. The result is a technique for calculating the effective permeability and permittivity of congregate material with arbitrary, intrinsic granular permeability and permittivity as a func-

tion of the product $ka=\sigma_0$ and the packing density.

Although the multipolar expansion is correct for all size-to-wavelength ratios, the Clausius-Mossotti relationship is not; its derivation includes putting the electric-field intensity equal to the gradient of a scalar potential function. Since the gradient relationship is correct only in the limit of zero frequency, interaction effects as calculated are applicable only at zero frequency. However, asymptotic results are very close to reality so long as particles remain small compared with the wavelength; that is, so long as

$$ka<1.0 . \tag{1}$$

Since our results are intended to apply to polycrystalline solids at microwave frequencies (or to aerosols at optical frequencies), we are interested in conditions under which Eq. (1) is applicable, although Lewin[6] has shown that theory and experiment are in good agreement up to approximately $ka\approx 1.0$. Although Eq. (1) is applicable to the problems of interest here, the permittivity and permeability of the grains may be large enough to make $k_i a$ large so that $k_i a > ka$. Since external moments of order n are proportional to $(ka)^{2n+1}$ higher-order moments remain small. Therefore, as with other theories, we keep only the dipole terms. Since for large and changing values of $k_i a$ the spherical Hankel function remains fixed in magnitude and varies rapidly in phase, so do the dipole moments and, in turn, so do their contribution to the external constitutive parameters. An exact accounting for the frequency-dependent phase both of μ and ϵ forms the theory presented in this paper.

II. CALCULATION MODEL

We solve for the field coefficients by expanding all fields, interior and exterior, by a multipolar field expansion,[13–15] and matching boundary conditions at the surface of the sphere. To help clarify the physical significance of the field coefficients, we consider the radial terms of the field expansions. Although the angular terms are required for solving the boundary conditions, they are derivable from the radial terms,[16] as detailed in our earlier work; we follow our previous notation.

Using a $e^{i\omega t}$ time dependence, we consider a z-directed, x-polarized plane wave incident upon the surface of a sphere of radius a centered at the origin. By definition, $\sigma=kr$, where r is the distance from the origin. $j_n(\sigma)$ and $h_n(\sigma)$ are, respectively, spherical Bessel functions and spherical Hankel functions of the second kind (also known as Riccati-Bessel functions). Associated Legendre functions of order n and degree one are given by $P_n^1(\cos\theta)$. Using rationalized mks units, the radial terms of the multipolar field expansion of the incident wave as defined are

$$\begin{aligned} E_r &= \sum_{n=1}^{\infty} i^{1-n}(2n+1)\frac{j_n(\sigma)}{\sigma}P_n^1(\cos\theta)\cos\phi , \\ \eta_o H_r &= \sum_{n=1}^{\infty} i^{1-n}(2n+1)\frac{j_n(\sigma)}{\sigma}P_n^1(\cos\theta)\sin\phi . \end{aligned} \tag{2}$$

The scattered fields are given by

$$\begin{aligned} E_r &= \sum_{n=0}^{\infty} i^{1-n}D_n n(n+1)\frac{h_n(\sigma)}{\sigma}P_n^1(\cos\theta)\cos\phi , \\ \eta_o H_r &= \sum_{n=0}^{\infty} i^{1-n}C_n n(n+1)\frac{h_n(\sigma)}{\sigma}P_n^1(\cos\theta)\sin\phi , \end{aligned} \tag{3}$$

where C_n and D_n form the infinite set of field coefficients.

For a description of the fields inside the sphere, we let σ_i represent the product of the internal wave vector k_i and radial distance r, where r is less than or equal to the sphere radius. The interior fields with this polarization are

$$\begin{aligned} E_r &= \sum_{n=0}^{\infty} i^{1-n}B_n n(n+1)\frac{j_n(\sigma_i)}{\sigma_i}P_n^1(\cos\theta)\cos\phi , \\ \eta H_r &= \sum_{n=0}^{\infty} i^{1-n}A_n n(n+1)\frac{j_n(\sigma_i)}{\sigma_i}P_n^1(\cos\theta)\sin\phi , \end{aligned} \tag{4}$$

where A_n and B_n form an infinite set of field coefficients. Matching boundary conditions, we find the scattering coefficients for the TE and TM fields, C_n and D_n, respectively, to be given by[2,14,17]

$$\begin{aligned} C_n &= \frac{2n+1}{n(n+1)}\frac{j_n(\sigma_i)J_n(\sigma_o)\eta - j_n(\sigma_o)J_n(\sigma_i)}{J_n(\sigma_i)h_n(\sigma_o)-j_n(\sigma_i)H_n(\sigma_o)\eta} , \\ D_n &= \frac{2n+1}{n(n+1)}\frac{j_n(\sigma_o)J_n(\sigma_i)\eta - j_n(\sigma_i)J_n(\sigma_o)}{j_n(\sigma_i)H_n(\sigma_o)-J_n(\sigma_i)h_n(\sigma_o)\eta} , \end{aligned} \tag{5}$$

where $\sigma_i=k_i a$ and $\sigma_o=ka$. The spherical Bessel and Hankel functions are given by

$$\begin{aligned} j_1(\sigma) &= \sin\sigma/\sigma^2-\cos\sigma/\sigma , \\ h_1(\sigma) &= e^{-i\sigma}(-1/\sigma+i/\sigma^2) . \end{aligned} \tag{6}$$

The derivative functions $J_1(\sigma)$ and $H_1(\sigma)$ are defined by

$$H_1(\sigma)=\frac{1}{\sigma}\frac{d}{d\sigma}(\sigma h_1(\sigma)) \tag{7}$$

These field coefficients are exact, and valid for all frequencies.

As previously stated, $k_i a$ can be any value but ka remains small; for this case, the expression for D_n is

$$D_n=\frac{i\sigma_o^{2n+1}}{n(n+1)[(2n-1)!!]^2}\frac{\eta\sigma_o J_n(\sigma_i)-(n+1)j_n(\sigma_i)}{nj_n(\sigma_i)-\eta\sigma_o J_n(\sigma_i)} . \tag{8}$$

The first fraction decreases rapidly with increasing value of n: $i\sigma_o^3/2, i\sigma_o^5/54, i\sigma_o^7/2700$, etc. The second fraction does not change much. In other words, all external fields created by higher-order terms are negligibly small. Our results are caused by changes in the external dipole moment.

The dipolar field coefficients are

$$C=\frac{3}{2}\frac{j_1(\sigma_i)J_1(\sigma_o)\eta-j_1(\sigma_o)J_1(\sigma_i)}{J_1(\sigma_i)h_1(\sigma_o)-j_1(\sigma_i)H_1(\sigma_o)\eta}\ ,$$
$$D=\frac{3}{2}\frac{j_1(\sigma_o)J_1(\sigma_i)\eta-j_1(\sigma_i)J_1(\sigma_o)}{j_1(\sigma_i)H_1(\sigma_o)-J_1(\sigma_i)h_1(\sigma_o)\eta}\ . \tag{9}$$

Approximate forms of the field coefficients have been used to determine the effective properties,[4,6] for $k_i a \ll 1$, Eq. (9) reduces to

$$C=-i\sigma_o^3\frac{\mu-1}{\mu+2}\ ,$$
$$D=-i\sigma_o^3\frac{\epsilon-1}{\epsilon+2}\ . \tag{10}$$

The approximate forms of the field coefficients result in calculation of an effective permeability (C) independent of grain permittivity, and an effective permittivity (D) independent of the grain permeability. To show how the permeability and permittivity are interrelated, we keep the next-order correction term for C and D to find

$$C\approx-i\sigma_o^3\frac{\mu-1}{\mu+2}-3i\sigma_o^5\frac{\epsilon\mu^2+\mu^2-6\mu+4}{10(\mu+2)^2}+\cdots\ ,$$
$$D\approx-i\sigma_o^3\frac{\epsilon-1}{\epsilon+2}-3i\sigma_o^5\frac{\mu\epsilon^2+\epsilon^2-6\epsilon+4}{10(\epsilon+2)^2}+\cdots\ . \tag{11}$$

The field coefficients are symmetrical with respect to μ and ϵ.[18,19] In Sec. III A we consider the difference between spectra calculated using the exact and approximate forms of the field coefficients.

The Clausius-Mossotti relation shows the effective permeability and permittivity to be[20,17]

$$\mu_{\text{eff}}=\frac{3\sigma_o^3+i8\pi a^3CN}{3\sigma_o^3-4i\pi a^3CN}\ , \tag{12}$$

$$\epsilon_{\text{eff}}=\frac{3\sigma_o^3+i8\pi a^3DN}{3\sigma_o^3-i4\pi a^3DN}\ , \tag{13}$$

where N is the number of spheres (grains) per unit volume. Doyle[2] uses an equivalent form of Eq. (13) to find the reflectance of a suspension of Ag spheres, with $\mu=1$. For close-packed, face-centered-cubic lattices, $N=1/(4a^3\sqrt{2})$, and

$$\mu_{\text{eff}}=\frac{3\sigma_o^3\sqrt{2}+i2\pi C}{3\sigma_o^3\sqrt{2}-i\pi C}\ , \tag{14}$$

$$\epsilon_{\text{eff}}=\frac{3\sigma_o^3\sqrt{2}+i2\pi D}{3\sigma_o^3\sqrt{2}-i\pi D}\ . \tag{15}$$

Equations (14) and (15) show the effective properties to be functions of μ and ϵ of the grain, and σ_o.

III. CALCULATED EFFECTIVE SPECTRA

We now use Eqs. (14) and (15) to calculate the effective permittivity and permeability spectra for different grain properties. In Sec. III A we compare spectra calculated using exact and approximate forms of the field coefficients. In Sec. III B we examine spectra calculated for several different constant sphere properties as a function of σ_o, and in Sec. III C we consider spectra calculated for frequency-dependent sphere properties. Most material applications are designed for a particular frequency range. Therefore, instead of changing our spectrum window to observe the dynamic responses for given sphere properties, we keep the window fixed and change the sphere properties to bring the dynamics into the window.

A. Field coefficient form

The coefficients C and D are evaluated at the surface of the sphere where $\sigma_i=\sigma_o\sqrt{\mu\epsilon}$. Small argument approximations are often used in scattering problems, even though the product $\sqrt{\mu\epsilon}$ of the reflecting material can be large; therefore, differences between the effective spectra calculated using exact and approximate forms of the field coefficients are of particular interest.

Figure 1 is a plot of μ_{eff} calculated with $\mu=250-i10$ and $\epsilon=15-i5000$ over the range $\sigma_o=10^{-4}$–10^{-1} using both exact and approximate forms of the field coefficients. $\sigma_i/\sigma_o=776.1-i805.4$. The permittivity and permeability values assigned the sphere are typical of those found in ferrites. The effective permeability calculated using the approximate form of the field coefficient shows a constant valued spectrum: μ'_{eff}, the dashed line in Fig. 1, is about 9.4 and μ''_{eff} is close to zero. The spectrum calculated using the exact form of the field coefficient is noticeably different. It is apparent that, although we restrain ourselves to a range where ka is small, the approximate form of the field coefficients leads to substantially different results when the internal wavelength is large. We use the exact form of the field coefficients for all remaining spectra calculations.

Figure 1 is worthy of note for it displays a μ_{eff} relaxation spectrum, much like the type measured experimentally,[21] which is not necessarily predicted using an electromagnetic torque equation. Absence of a negative value is ascribed to field averaging over multidirected and shaped units, although such averaging will always pro-

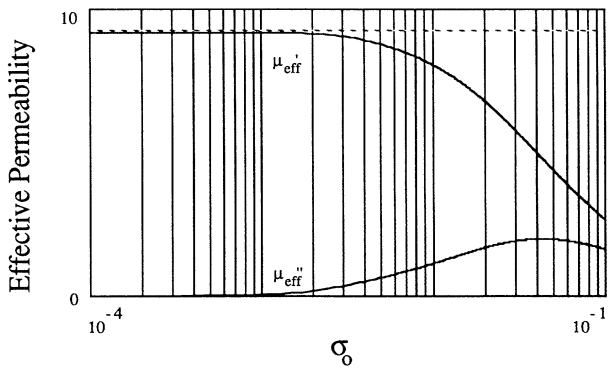

FIG. 1. μ_{eff} calculated for $\mu=250-i10$ and $\epsilon=15-i5000$ using exact form of field coefficient given in Eq. (9). Dashed line is μ'_{eff} calculated using approximate form of field coefficient given in Eq. (10). $\sigma_i/\sigma_o=776.1-i805.4$. The σ_o range is from 10^{-4} to 10^{-1}.

duce a μ' less than 1 at high frequencies.[7,22] Figure 1 demonstrates that this type of spectrum also arises from granular size effects. Postulates about atomic scale properties or polycrystalline averaging are unnecessary.

B. Fixed grain properties

In this section we investigate the effects on the conglomerate spectra of assigning the individual spheres different constant valued permittivities and permeabilities. The values assigned to the individual spheres are chosen to clearly present the dependence of the effective property spectra and not to necessarily reflect actual materials.

We begin by considering the effects of changing μ' of the sphere while keeping μ'' and the permittivity constant. Figure 2 shows μ_{eff} calculated for $\mu=5000-i2$ and $\epsilon=200\,000-i10\,000$. The μ_{eff} plot shows a relaxation, while the ϵ_{eff} spectrum calculated for the same values is flat. Larger values of μ' act to shift the relaxation point of μ_{eff} to lower values of σ_o and increase that of ϵ_{eff}. Figure 3 is a plot of μ_{eff} with μ' changed to 5. We see a classical resonance response where μ'_{eff} goes negative and μ''_{eff} peaks at the midpoint of the μ'_{eff} slope, but with "feet" at the tail end of the traces. Such feet are prevalent in measured experimental work[7,8,10] and have been the subject of much discussion.[7,10,11,22]

Figure 3 shows a μ_{eff} spectrum quite similar to that measured and discussed by Rado *et al.*[10] They ascribed a similar spectrum with multiple peaks to the combination of two different, microscopic permeability mechanisms: wall motion and coherent domain rotation. They attempted to separate the two mechanisms by milling the material to a smaller grain size which they hypothesized would eliminate domain-wall movement. After the material has been remilled to a smaller particle size, the multiple peaks were not present, which they took as proof that the multiple peaks of the spectrum were from the combination of different permeability mechanisms. Although other evidence shows that the conclusions drawn by Rado *et al.* in their paper may be correct,[10] Fig. 3 demonstrates that such complex spectra are obtainable from a single mechanism.

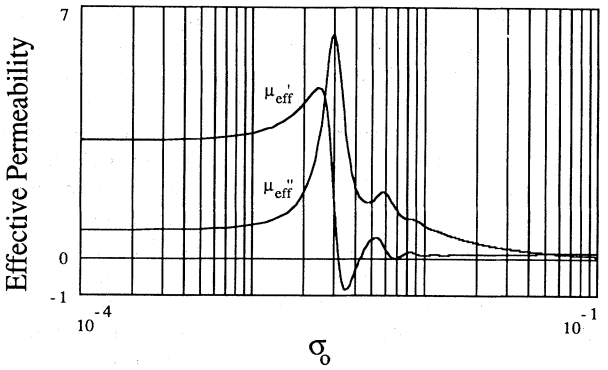

FIG. 3. μ_{eff} calculated for $\mu=5-i2$ and $\epsilon=200\,000-i10\,000$. The σ_o range from 10^{-4} to 10^{-1}.

Figure 4 is a plot of μ_{eff} calculated using $\mu=5-i20$ and $\epsilon=200\,000-i10\,000$. The μ_{eff} spectrum is quite different from that seen in Fig. 3, where $\mu=5-i2$. The steps evident in Fig. 3 have disappeared into a slowly damped tail, while ϵ_{eff} is little changed. Increasing μ'' produces a lower Q resonance with the resonance shifted to a higher frequency; ϵ_{eff} changes slightly to indicate a lower resonance frequency.

C. Frequency-dependent grain properties

We now consider the effective spectra when the permeability and permittivity of the grains are frequency dependent. We determine the dynamic, frequency-dependent permeability of the grain using the Gilbert equation[8] given by

$$\frac{d\mathbf{M}}{dt}=\gamma(\mathbf{M}\times\mathbf{H})-\frac{\alpha}{4\pi M_s}\left[\mathbf{M}\times\frac{d\mathbf{M}}{dt}\right], \tag{16}$$

where the boldface type signifies vectors. $\mathbf{M}$ represents the magnetization, $4\pi M_s$ the saturation magnetization, and $\mathbf{H}$ is the magnetic field. γ is the gyromagnetic ratio taken as 2.8 MHz/Oe. α is the damping coefficient, equal

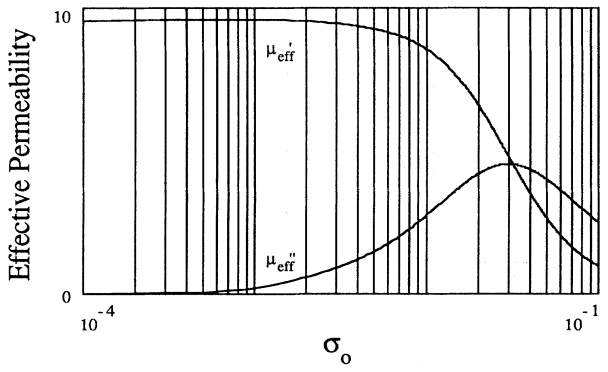

FIG. 2. μ_{eff} calculated for $\mu=5000-i2$ and $\epsilon=200\,000-i10\,000$. The σ_o range is from 10^{-4} to 10^{-1}.

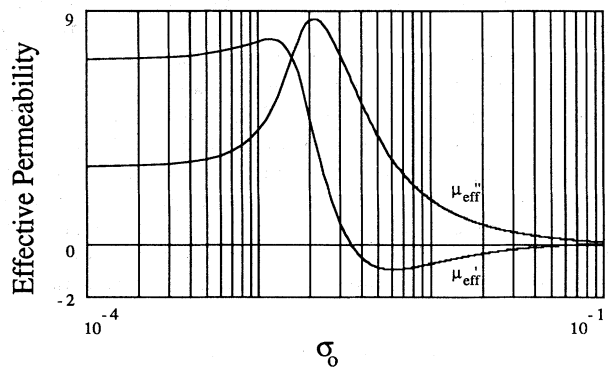

FIG. 4. μ_{eff} calculated for $\mu=5-i20$ and $\epsilon=200\,000-i10\,000$. The σ_o range is from 10^{-4} to 10^{-1}.

to, approximately, several tenths for highly damped materials, 10^{-2} for thin films, and 10^{-3} for single crystals. The magnetization $\mathbf{M}$ is the vector sum of the saturation magnetization $4\pi\mathbf{M}_s$ and the rf magnetization. Similarly, the magnetic field vector $\mathbf{H}$ is the vector sum of all internal fields acting on the magnetization, which includes the externally applied field $\mathbf{H}_0$, the shape demagnetizing field, the anisotropy field H_k, and the rf magnetic field.

Our analysis is applicable to two special cases: One is where the magnetic moment of each sphere, summed over its contained domains, is zero; the other is for single-domain, randomly oriented spheres, the macroscopic moment of which sums to zero. As $k_i a$ increases, the fields interior to the sphere become more position dependent. Our extension to include frequency-dependent, non-uniform internal-field distributions increases the channel for power transfer from the uniform precessional mode to Walker modes. However, our analysis is limited to small-signal permeabilities, where the rf applied field is vanishingly small, and so we ignore power losses other than those described by the loss term of Eq. (16). As previously discussed, so long as there is no external static moment, the off-diagonal terms sum to zero and can be neglected:[11] The result is that the permeability of the ensemble is a scalar quantity. With use of Eq. (16), the relative sphere permeability is found to be

$$\mu=\frac{\omega_m(\omega_m+i\omega\alpha)}{(\omega_k+i\omega\alpha)(\omega_0+i\omega\alpha)-\omega^2}+1, \tag{17}$$

where $\omega_m=\gamma 4\pi M_s, \omega_k=\gamma H_k, \omega_0=\gamma H_0$, and ω is the signal frequency.

For microwave-to-millimeter wave frequencies the complex permittivity of the sphere is commonly modeled using free-electron theory.[23] For these frequencies the sphere permittivity is approximated by

$$\epsilon_r=\epsilon'-i/\rho\epsilon_0\omega\ , \tag{18}$$

where ρ is the resistivity. In this section we shall consider the effective property spectra while using, respectively, Eqs. (17) and (18) for calculation of the grain permeability and permittivity. We examine changes in the effective spectra due to variation of five different grain properties: sphere radius a, ϵ', ϵ'' via the resistivity ρ, damping coefficient α, and crystalline anisotropy H_k.

The resonance frequency predicted using the Gilbert equation is approximated by $f_r \approx \gamma\sqrt{4\pi M_s H_k}$, and the initial permeability by $4\pi M_s/H_k$. Since the two variables, M_s and H_k, are interrelated we do not consider the effective spectra as a function of the saturation magnetization. The spectra are presented as a function of frequency to provide a better intuitive feeling on how changes in the frequency-dependent grain properties affect the calculated spectra. We keep the frequency range between 10 MHz and 10 GHz, and examine variable effects on the response inside the frequency window.

1. *Variable grain radius*

We now consider the dependence of the effective spectra upon particle size. Equation (17) is used to determine the permeability of the grain with $4\pi M_s=10^4$ G, $\alpha=0.15$, and $H_k=10.0$ Oe. Equation (18) is used to calculate grain permittivity with $\epsilon'=5$, and $\rho=10^5$ Ω m. Figure 5 is a plot of μ_{eff} for grain size $a=10^{-5}$ m. For these particular grain values the μ_{eff} spectrum remains virtually unchanged for grain size ranging between 10^{-7} and 10^{-2} m, although the responses do have slightly lower Q's, lower resonance frequencies, and decreased magnitudes as the particle size is increased.

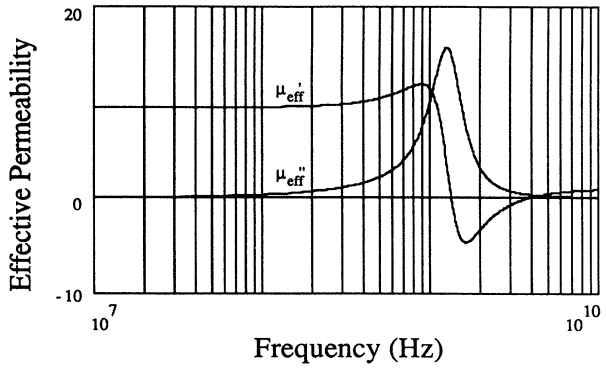

FIG. 5. μ_{eff} calculated for grain properties $H_k=10.0$ Oe, $\alpha=0.15$, $4\pi M_s=10^4$ G, $\epsilon'=5$, and $\rho=10^5$. $a=10^{-5}$ m. The frequency range is 10 MHz to 10 GHz.

For grain sizes below 10^{-4} m, the ϵ_{eff} spectrum is constant valued; ϵ'_{eff} is about 9.5 and ϵ''_{eff} is of negligible value. As the grain size increases beyond 10^{-4} m, a relaxation appears in the ϵ_{eff} spectrum which shifts to lower frequencies as particle size is increased. Small changes in the particle size dramatically affect the shape of the calculated spectrum. Figure 6 shows ϵ_{eff} calculated for a grain size of 10^{-2} m. The spectrum is a complex one, similar to those measured for some $NiFe_2O_4$ ferrites,[9] for which no theory has been put forth to explain. Increasing or decreasing the conductivity of the grains acts to enhance or reduce the rise in ϵ'_{eff} prior to resonance.

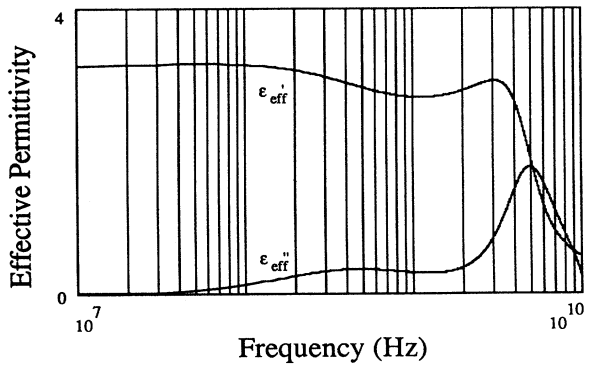

FIG. 6. ϵ_{eff} calculated for grain properties $H_k=10.0$ Oe, $\alpha=0.15$, $4\pi M_s=10^4$ G, $\epsilon'=5$, and $\rho=10^5$. $a=10^{-2}$ m. Frequency range is 10 MHz to 10 GHz.

2. Variable ϵ'

We now consider the effect of changing ϵ' of the grain. The sphere permeability is determined using Eq. (17) with $H_k = 10.0$ Oe, $\alpha = 0.15$, and $4\pi M_s = 10^4$ G. $a = 10^{-5}$ m. The sphere permittivity is determined using Eq. (18) with $\rho = 10^{-3}$ Ω m. Figure 7 shows μ_{eff} calculated with ϵ' of the grain set equal to 1. The spectrum shows a classical resonance. The calculated ϵ_{eff} spectrum is virtually constant with ϵ'_{eff} about 9.5, and ϵ''_{eff} increases with frequency but is still quite small, 0.06, at 10 GHz. Keeping in mind that ϵ' values larger than a few tens are plausible only for bulk ferroelectric materials we find that the spectra remain virtually the same for ϵ' up to, approximately, 10^5. Figure 8 is a plot of μ_{eff} calculated with $\epsilon' = 5 \times 10^6$. The spectrum displays a second resonance of reduced magnitude at a higher frequency. Such second resonance tails have been measured, and predicted using a macroscopic (sample size) dimensional resonance theory.[24] Figure 8 demonstrates that the same type of secondary resonance can be obtained from a microscopic basis. The second resonance is seen between $\epsilon' \approx 2 \times 10^6$ and 2×10^7. While the frequency of the first resonance stays constant, the frequency and spectral magnitude of the second resonance shift lower with the increase in ϵ'. At $\epsilon' = 10^7$, a third resonance peak is visible. Further increases in ϵ' bring the μ_{eff} spectra back to the classical form of the resonance curve and begin to lower the resonance frequency. The ϵ_{eff} spectrum remains unchanged for ϵ' values up through 10^{10}.

3. Variable ϵ''

We now consider the effect of changing ϵ'' of the grain. The grain permeability is calculated with $4\pi M_s = 10^4$ G, $\alpha = 0.15$, and $H_k = 10.0$ Oe. $a = 10^{-4}$ m, and $\epsilon' = 5$. For small values of resistivity, $\rho < 10^{-4}$ Ω m, the μ_{eff} spectrum displays a relaxation. As the resistivity is increased from 10^{-4} to 10^0 Ω m, the resonance sharpens, dropping all vestiges of a relaxation. For ρ values greater than 10^0 Ω m, the μ_{eff} spectrum is quite similar to that seen in Fig. 7.

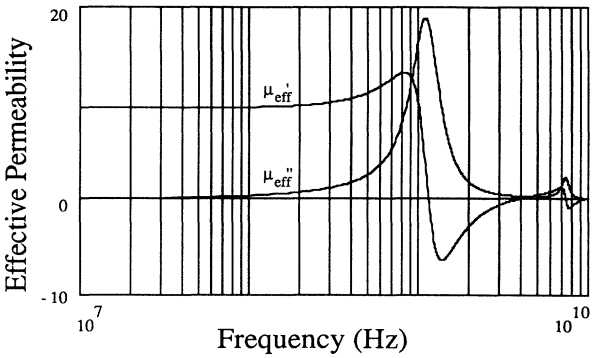

FIG. 8. μ_{eff} calculated for grain properties $H_k = 10.0$ Oe, $\alpha = 0.15$, $4\pi M_s = 10^4$ G, $\rho = 10^{-3}$, and $a = 10^{-5}$ m. $\epsilon' = 5 \times 10^6$. Frequency range is 10 MHz to 10 GHz.

For $\rho < 10^{-2}$ Ω m, the ϵ_{eff} spectrum is constant, showing no signs of a resonance; ϵ'_{eff} is about 9.5, and ϵ''_{eff} is of negligible value. At $\rho = 10^{-2}$, the spectrum changes from one of constant value to one indicating the onset of a relaxation or resonance. As the resistivity is further increased, the relaxation shifts to lower frequencies inside the window. Figure 9 is a plot of ϵ_{eff} calculated for $\rho = 10^0$. As the resistivity is further increased, the relaxation shifts to frequencies below the limits of the plot; ϵ''_{eff} goes to zero, and ϵ'_{eff} goes to approximately 4.5.

4. Variable damping coefficient

We now consider the effect of changing the damping coefficient of the grain. Equation (17) determines sphere permeability with $4\pi M_s = 10^4$ G and $H_k = 10.0$ Oe. Equation (18) determines the sphere permittivity with $\rho = 10^{-3}$ Ω m and $\epsilon' = 10$. $a = 10^{-5}$ m. Figure 10 is a plot of μ_{eff} calculated with $\alpha = 0.015$. The μ_{eff} spectrum shows a sharp resonance of large magnitude much like those associated with single crystals. The ϵ_{eff} spectrum is constant over the frequency range with ϵ'_{eff} equal to ap-

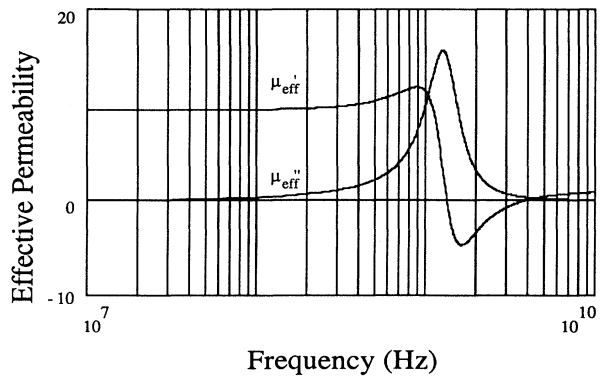

FIG. 7. μ_{eff} calculated for grain properties $H_k = 10.0$ Oe, $\alpha = 0.15$, $4\pi M_s = 10^4$ G, $\rho = 10^{-3}$, and $a = 10^{-5}$ m. $\epsilon' = 1$. Frequency range is 10 MHz to 10 GHz.

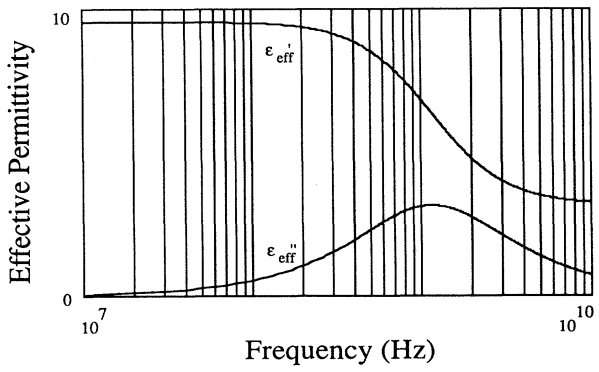

FIG. 9. ϵ_{eff} calculated for grain properties $H_k = 10.0$ Oe, $\alpha = 0.15$, $4\pi M_s = 10^4$ G, $\epsilon' = 5$, and $a = 10^{-4}$ m. $\rho = 1$. Frequency range is 10 MHz to 10 GHz.

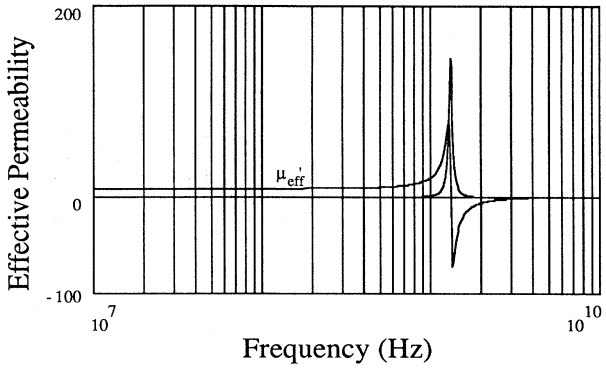

FIG. 10. μ_{eff} calculated for grain properties $H_k = 10.0$ Oe, $4\pi M_s = 10^4$ G, $\rho = 10^{-3}$, $\epsilon' = 10$, and $a = 10^{-5}$ m. $\alpha = 0.015$. Frequency range is 10 MHz to 10 GHz.

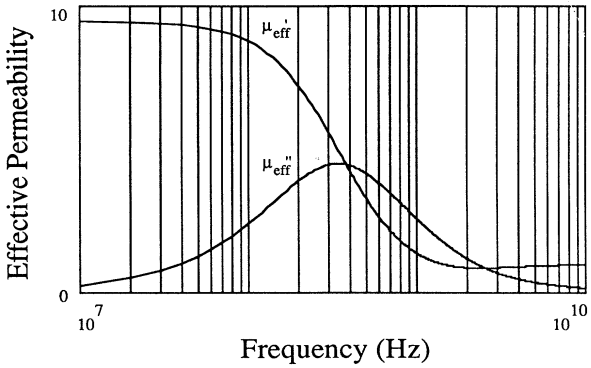

FIG. 12. μ_{eff} calculated for grain properties $H_k = 10.0$ Oe, $4\pi M_s = 10^4$ G, $\rho = 10^{-3}$, $\epsilon' = 10$, and $a = 10^{-5}$ m. $\alpha = 1.20$. Frequency range is 10 MHz to 10 GHz.

proximately 9.6 and ϵ_{eff}'' of negligible value but increasing with frequency.

Figure 11 is a plot of μ_{eff} calculated for $\alpha = 0.15$. The spectrum has relaxed with the increase in damping coefficient, with resonance no longer such a sharp transition. The resonance frequency has shifted slightly downward, and the spectral magnitudes at resonance have decreased by a factor of about 10. The ϵ_{eff} spectrum is virtually unchanged from that calculated with the smaller damping coefficient.

Figure 12 is a plot of μ_{eff} calculated for $\alpha = 1.20$. The μ_{eff} resonance has become a relaxation, with μ_{eff}'' showing a very wide resonance peak. μ_{eff}' no longer goes negative. Greater spectra relaxation is seen for further increases in the damping coefficient; μ_{eff}' stays positive, and the resonance frequency shifts to values below 10 MHz. The ϵ_{eff} spectrum remains the same, appearing to be unaffected by the value of the damping coefficient within the frequency range examined.

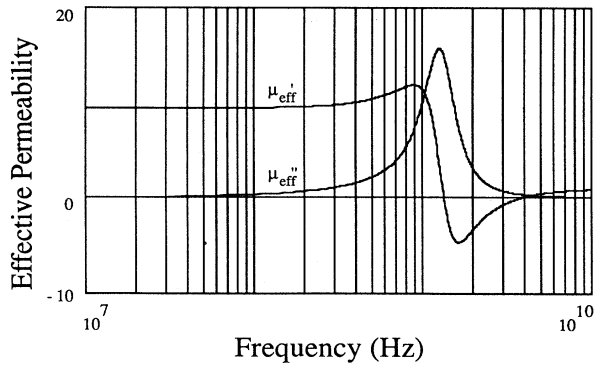

FIG. 11. μ_{eff} calculated for grain properties $H_k = 10.0$ Oe, $M_s = 10^4$ G, $\rho = 10^{-3}$, $\epsilon' = 10$, and $a = 10^{-5}$ m. $\alpha = 0.15$. Frequency range is 10 MHz to 10 GHz.

5. *Variable H_k*

We examine the effect of the crystalline anisotropy using Eq. (17) to determine the grain permeability for $4\pi M_s = 10^4$ G and $\alpha = 0.15$, and using Eq. (18) to determine the grain permittivity with $\epsilon' = 10$ and $\rho = 10^{-3}$, and $a = 10^{-5}$ m. We find, for a range of anisotropy values from 0.01 to 200 Oe, a μ_{eff} spectrum almost identical to that of Fig. 11, and a constant valued ϵ_{eff} spectrum with ϵ_{eff}' equal to about 9.5 and ϵ_{eff}'' about 0. For these grain values the crystalline anisotropy seems to have little effect on the calculated spectra.

IV. DISCUSSION AND CONCLUSIONS

This work considers the effective permeability and permittivity spectra of polycrystalline materials. In particular it addresses the dependence of macroscopic values on the intragranular values of grain permeability and permittivity and upon the size-to-wavelength ratio. To do this, we first calculate the scattering from an isolated sphere of arbitrary material. An infinite, cubic array of such spheres is then used to form the polycrystalline solid. Sphere-sphere interaction is accounted for by using the Clausius-Mossotti relationship. Since the Clausius-Mossotti relationship is valid only for small external-size–to–wavelength ratios, our results are applicable only to that case.

Attempts have been made to explain permeability spectra displaying multiple peaks or relaxations by summing a resonant response over a range of grain parameters.[7,10,22] This approach fails, however, since a resonant microscopic model leads to a resonant macroscopic one. The local field, particularly when the internal wavelength is large, must be considered. The theory presented here results in spectra that match measured resonances and also predicts, under appropriate conditions, other more anomalous permeability and permittivity spectra that have been experimentally observed. Our results suggest that it is necessary to include the effects of the in-

tragranular size to wavelength ratio as well as the Clausius-Mossotti equations if spectra are to be properly interpreted.

We find that high-permittivity spheres give an ϵ_{eff} that primarily measures the volume fraction occupied by the spheres, and, depending upon the size of the sphere, that the permittivity may strongly influence the μ_{eff} spectrum. Dual comments are, of course, valid. When the permittivity and permeability of the sphere are large, the spectra obtained using the approximate and exact forms of the field determining coefficients are quite different.

Section III B shows that the familiar frequency-dependent spectra can be obtained from a lattice composed of grains with constant properties. With μ'', ϵ', and ϵ'' kept fixed, different, constant values of μ' result in effective permeability spectra ranging from resonance to relaxation. Changing μ'' while keeping μ', ϵ', and ϵ'' fixed varies the Q of the spectra.

Section III C considers the effective spectra calculated for a lattice of spheres with frequency-dependent electromagnetic properties. The sphere permeability was determined using the Gilbert equation, and the sphere permittivity determined using free-electron theory. Section III C 1 shows that the sphere size plays a large role in determining the effective spectra. Results include spectra quite similar to published data considered to be anomalous. Section III C 2 shows that changing ϵ' had little effect on the calculated effective spectra. Although increasing ϵ' did shift the resonance frequency slightly lower, the effect was not noticeable for realistic values of ϵ'.

In Sec. III C 3 we saw that varying ϵ'' produces a dramatic change in the calculated effective permeability spectra. Larger values of ϵ'' produce relaxations common to low-frequency ferrites while smaller ϵ'' values produce resonances typical of single crystals. Section III C 4 shows that changing the damping coefficient α of the sphere greatly affects the effective permeability spectra. At small values of α, the calculated spectra resembled those typical of a single crystal, while large α values resulted in lower-Q responses. Section III C 5 shows that changing the anisotropy field H_k of the sphere has little effect on the calculated effective spectra.

One series of permeability spectra seen in the paper by Miles *et al.*[9] is particularly interesting for comparison to results calculated in this work; they display a series of temperature-dependent permeability spectra measured at 298, 153, and 83 K for four different nickel-zinc ferrites. Their temperature-dependent spectra correspond quite closely to those of Sec. III C 1: effective spectral dependence upon the size of the spheres. The temperature dependence can be simply explained if the constituent parameters of the grain changed with temperature.

Dimensional resonance effects on permeability and permittivity spectra have been examined from a macroscopic point of view which considers both the physical size and shape of the sample being measured. Brockman *et al.*. investigated macroscopic dimensional effects in a high-permittivity ferrite.[24] They developed a theory to predict μ_{eff} and ϵ_{eff} spectra as a function of the bulk material properties and physical dimensions of the sample being measured. Their predicted spectra are similar to some presented in this work calculated from a microscopic basis. Analogous to the work described here, these authors point out that the frequency-dependent μ_{eff} and ϵ_{eff} spectra which their theory predicts are not necessarily determined by dispersion of the bulk material making up the sample; similar spectra are obtained using constant-valued material. Although dimensional effects are well accepted on a macroscopic basis, there has been little work considering the effect on a microscopic level. Results presented here suggest that the role of dimensional resonance between the microscopic particles in determining the permeability and permittivity spectra need to be considered.

An extended method of calculating the permeability and permittivity spectra of composite materials has been introduced that includes dimensional effects on a granular level. The ability of the method to calculate many different, complex spectra from a single origin is noteworthy. Our work suggests that the frequency dependence of the permeability and permittivity spectra is strongly affected by dimensional responses at the granular level.

ACKNOWLEDGMENTS

The authors thank Professor E. L. Hixson of The University of Texas for his support of this work.

[1]L. D. Landau and E. M. Lifshitz, *Electrodynamics of Continuous Media* (Pergamon, New York, 1960).
[2]W. T. Doyle, Phys. Rev. B **39**, 9852 (1989).
[3]H. R. D. Sunak and S. P. Bastien, IEEE Photon. Tech. Lett. **1**, 142 (1989).
[4]D. Stroud and F. D. Pan, Phys. Rev. B **17**, 1602 (1978).
[5]P. Sheng, Phys. Rev. Lett. **45**, 60 (1980).
[6]L. Lewin, Trans. IRE **94**, Part III, 65 (1946).
[7]J. Smit and H. P. J. Wijn, *Ferrites* (Wiley, New York, 1959).
[8]B. Lax and K. J. Button, *Microwave Ferrites and Ferrimagnetics* (McGraw-Hill, New York, 1962).
[9]P. A. Miles, W. B. Westphal, and A. Von Hippel, Rev. Mod. Phys. **29**, 279 (1957).
[10]G. T. Rado, R. W. Wright, and W. H. Emerson, Phys. Rev. **80**, 273 (1950).
[11]D. M. Grimes, Phys. Chem. Solids **3**, 141 (1957).
[12]D. M. Grimes, R. D. Harrington, and A. L. Rasmussen, Phys. Chem. Solids **12**, 28 (1959).
[13]W. K. H. Panofsky and M. Phillips, *Classical Electricity and Magnetism* (Addison-Wesley, New York, 1962).
[14]J. A. Stratton, *Electromagnetic Theory* (McGraw-Hill, New York, 1941).
[15]See, for example, H. C. Van de Hulst, *Light Scattering by Small Particles* (Wiley, New York, 1957).
[16]D. M. Grimes, J. Math. Phys. **23**, 897 (1982).
[17]C. A. Grimes, Doctoral dissertation, The University of Texas

at Austin, 1990, University Microfilms, 300 N. Zeeb Road, Ann Arbor, MI 48106.
[18]G. A. Niklasson and C. G. Granqvist, J. Appl. Phys. **55**, 3382 (1984).
[19]F. Claro, Phys. Rev. B **30**, 4989 (1984).
[20]J. C. Maxwell Garnett, Philos. Trans. R. Soc. London **203**, 385 (1904); **205**, 237 (1906).
[21]C. A. Grimes, J. Mag. Mag. Mater. **80**, 165 (1989).
[22]D. Park, Phys. Rev. **97**, 60 (1955).
[23]S. Ramo, J. R. Whinnery, and T. Van Duzer, *Fields and Waves in Communication Electronics* (Wiley, New York, 1984).
[24]F. G. Brockman, P. H. Dowling, and W. G. Steneck, Phys. Rev. **77**, 85 (1950).